Jordanian Journal of Engineering and Chemical Industries

Print ISSN: 2616 - 9584 Online ISSN: 2617 - 720X

Atomistic Thermodynamics of Water over Actinide Oxide Surfaces: Implications on Stabilities and Morphologies

Niveen W. Assaf[1]*, Ibukun Oluwoye[2], Ali Marashdeh[3]and Ali Elrashidi[4,5]

[1]*Al-Balqa Applied University, Faculty of Engineering Technology, Chemical Engineering Department, Al Salt 19117, Jordan*

[2]*Curtin Corrosion Centre, Curtin University, GPO Box U1987, Perth, WA 6845, Australia.*

[3]*Department of Chemistry, Al-Balqa Applied University, Salt, Jordan.*

[4]*College of Engineering, University of Business and Technology, 21448 Jeddah, Saudi Arabia.*
[5]*Department of Engineering Physics, Alexandria University, Alexandria 21544, Egypt*

Highlights

- Stability of water over actinide oxides was revealed.
- Dissociative adsorption is predominant on (100) and (110) surfaces.
- (111) surfaces were found to have a stable mixed water layer.
- Nanoparticles will adopt octahedral and truncated-octahedral shapes in moist media.
- The study provides insights into corrosion and catalysis.

Abstract

The surface free energy diagrams of water adsorption on the low-index surfaces of UO_2 and PuO_2 were calculated using the ab initio atomistic thermodynamics technique. The phase diagrams of both UO_2(100) and PuO_2(100) surfaces show that the dissociative H-OH adsorption of water exhibits higher stability for all applied coverages. Chemical potential, with PuO_2(100) stabilizing hydroxylated structures at lower chemical potentials than UO_2(100). On the (110) surfaces, dissociative adsorption is also preferred, but with reduced reactivity compared to (100); UO_2(110) supports hydroxylation at lower chemical potentials than PuO_2(110), indicating a greater tendency for early-stage protonation. On the closed-packed (111) surfaces, the stability diagrams revealed that only a mixed monolayer containing both molecular and dissociated water becomes stable, and only under more humid or elevated temperature conditions. The mixed adsorption phase on PuO_2(111) becomes stable at a lower chemical potential relative to UO_2(111), indicating slightly higher reactivity. The equilibrium morphology of UO_2 and PuO_2 nanoparticles in humid environments were predicted using the Wulff construction. The results showed that the (111) facets dominate across the full range of water chemical potentials, yielding octahedral nanoparticles. For PuO_2, a transition to truncated octahedral was observed $\Delta\mu_{H_2O} = -0.50$ eV due to the emergence of (110) facets. These findings clarify the role of thermodynamic and kinetic variables affecting water interactions with actinide oxides, pertinent to corrosion, catalysis, and the performance of nuclear materials.

Paper type: Research Paper.

Keywords: uranium dioxide, plutonium dioxide, adsorption; DFT, wulff construction, stability, thermodynamic.

Citation: Assaf, N., W., Oluwoye, I., Marashdeh, A., and Elrashidi, A. "Atomistic thermodynamics of water over actinide oxide surfaces: implications on stabilities and morphologies" *Jordanian Journal of Engineering and Chemical Industries*, Vol. 8, No.2, pp:214-226 (2025).

* Corresponding author: E-mail: niveen.assaf@bau.edu.jo ORCID: https://orcid.org/0000-0002-5710-6282
Received 12 June 2025 Revised: 25 June 2025 Accepted 8July 2025
Jordanian Journal of Engineering and Chemical Industries (JJECI), Vol.8, No.2, 2025, pp: 214-226

1. Introduction

Uranium dioxide (UO_2) and plutonium dioxide (PuO_2) are widely used in the nuclear sector owing to their remarkable thermal stability, chemical durability, and radiation resistance.(Cozzo et al., 2011; Gibby, 1971; Pang et al., 2013; Vălu et al., 2014) Both oxides adopt a fluorite-type crystal structure,(Prodan et al., 2006) ensuring substantial structural stability even under extreme temperature and irradiation conditions. UO_2 is extensively utilized as a fuel in commercial nuclear reactors owing to its high melting point (~3078 K)(Hausner, 1965) and low thermal conductivity,(Lucuta et al., 1996) which facilitate the containment of fission products under operational conditions.(Eriksen et al., 2012) PuO_2, on the other hand, is used in mixed oxide (MOX) fuels, which combine UO_2 and PuO_2 for use in both thermal and fast reactors, therefore, enhancing fuel efficiency and facilitating plutonium recycling.(Kurosaki et al., 2001) UO_2 and PuO_2 demonstrate significant chemical stability under irradiation and extreme temperatures; however, their interaction with water and oxygen at the surface level may lead to corrosion,(Banos et al., 2021; Banos et al., 2018; Banos & Scott, 2020; Haschke, 1998; Wasywich et al., 1993) oxidation,(Haschke et al., 2001; McEachern & Taylor, 1998; Ritchie, 1981) defect formation,(Ao et al., 2015; Flores et al., 2011; Hernandez & Holby, 2016; Richmond et al., 2010) and phase transformation, potentially affecting fuel performance, chemical reactivity(Pacchioni, 2017; Papageorgiou et al., 2010; Reticcioli et al., 2017; Yim et al., 2018) and long-term storage stability.(Haschke et al., 2000; Haschke & Ricketts, 1997; Stakebake, 1971) Gaining insight into the surface chemistry of these substances is crucial for both fundamental research and technological applications,(Cui et al., 2011) as it influences multiple facets of the nuclear industry, including nuclear fuel corrosion,(Haschke et al., 2000; Skomurski et al., 2008) hydrogen gas production and release,(Baker et al., 1966; Jonsson et al., 2007) as well as the safe handling and long-term storage of spent fuels.(Haschke et al., 2000; Haschke & Ricketts, 1997; Stakebake, 1971) Moreover, gaining insight into the thermodynamics and kinetics of these processes is crucial for enhancing fuel design and accurately predicting fuel performance in actual reactor and storage environments.

Theoretical and experimental investigations align on a coherent understanding of H_2O-UO_2 and H_2O-PuO_2 interactions. Bo et al.(Bo et al., 2014) elucidated the atomic-level adsorption and dissociation behavior of water molecules on the (100), (110), and (111) surfaces of UO_2, demonstrating that the behavior of water adsorption is significantly influenced by surface orientation. On the (111) and (110) surfaces, water molecules and hydroxyl ions preferentially adsorb at the top of uranium sites, whereas on the (100) surface, they occupy the bridge sites between adjacent uranium atoms. Moreover, the UO_2 (100) surface has a greater propensity to adsorb both molecular and dissociative water than the UO_2 (111) and UO_2(110) surfaces, owing to its enhanced surface reactivity. They also found that at 0.25 ML coverage, the adsorption energy for molecular water on the UO_2(111) surface is comparable to that of dissociative adsorption, nevertheless, it is much less stable than dissociative adsorption on the UO_2(110) and UO_2(100) surfaces. They indicated that, as coverage rises, the adsorption energy of molecular water stays constant on the UO_2(111) and UO_2(100) surfaces, whereas dissociative adsorption diminishes, except on the UO_2(110) surface where adsorption energy remains steady.(Bo et al., 2014) Tegner et al.(Tegner et al., 2017) examined the interaction of molecular and dissociated water with low-index surfaces of UO_2 and PuO_2. Their study verified that both (110) and (100) exhibit considerable reactivity with water molecules, resulting in the formation of stable hydroxyl groups at 1 ML coverages, whereas the (111) surface displays a stable confirmation that encompasses both molecular and dissociative water behavior at the same coverage. Maldonado et al.(Maldonado et al., 2014) examined the temperature and pressure-dependent adsorption reactions of some flat and stepped UO_2 surfaces, specifically (111), (211), and (221), revealing that, at room temperature and ambient pressure, water consistently reacts with UO_2 surfaces, resulting in water dissociation and modifications to the step morphology. A comprehensive analysis of the behavior of excess electrons from intrinsic oxygen vacancies on actinide-oxide surfaces by Wang et al.(Wang et al., 2019) reveals that excess electrons localize very differently depending on the actinide: in the ThO_2 the electrons remain at the vacancy site, in PuO_2 they transition into Pu 5f orbitals; while UO_2 exhibits intermediate behavior. They have found that these localization differences significantly affect water chemistry on the surfaces; on ThO_2 and UO_2, vacancy-trapped electrons facilitate water adsorption and spontaneous dissociation (exothermic H_2O splitting) resulting in H_2 release, whereas on PuO_2 the delocalized electrons are ineffective in promoting H_2 evolution, rendering H_2 formation thermodynamically unfavorable. They ensure that this tendency results in differences in surface reactivity and catalytic behavior among the three dioxides, which have significant consequences for water-induced corrosion processes and the stability of nuclear fuel surfaces.

Experimental data from X-ray photoelectron spectroscopy (XPS) indicated that increased humidity leads to higher uranium oxidation states, with water first adsorbing in a molecular form and then converting to hydroxyl species with prolonged exposure.(Donald et al., 2016) Haschke et al.(Haschke et al., 2001) conducted experimental investigations on the interactions of PuO_2 with water using microbalance (MB) and pressure-volume-temperature (PVT) methods, demonstrating that water exhibits substantial adsorption below 393 K and desorption at about 473 K, with hydroxyl groups facilitating the oxidation of PuO_2 and the generation of H_2 in the presence of oxygen. Subsequent experimental studies have examined the interaction between water and uranium oxide surfaces,(Balooch & Hamza, 1996; Hedhili et al., 2000; Manner et al., 1999; Paffett et al., 2003; Senanayake & Idriss, 2004; Senanayake et al., 2005; Stultz et al., 2004; Tian et al., 2014) confirming that H_2 is produced by water dissociation on UO_2 surfaces.(Hedhili et al., 2000; Senanayake & Idriss, 2004; Senanayake et al., 2005) On stoichiometric UO_2(111) surfaces, H_2O exhibits modest interaction, with the majority of molecular adsorption at 300 K being reversible. In contrast, on reduced surfaces with oxygen vacancies, water adsorbs strongly via a dissociative process.(Senanayake & Idriss, 2004; Senanayake et al., 2005) Furthermore, water adsorption on stoichiometric surfaces

has no influence on surface oxidation, but reduced UO_2 surfaces undergo oxidation upon interaction with water.(Hedhili et al., 2000; Senanayake & Idriss, 2004; Stultz et al., 2004)

This study utilizes ab initio atomistic thermodynamics to compute surface free energy phase diagrams resulting from the interaction of water on the ideal, defect-free low-index UO_2 and PuO_2 surfaces. It shows the development of stability for various H_2O/UO_2 and H_2O/PuO_2 configurations throughout a broad spectrum of water coverages. It also ascertains the morphologies of uranium and plutonium oxides nanoparticles under varying water environments using the Wulff construction.

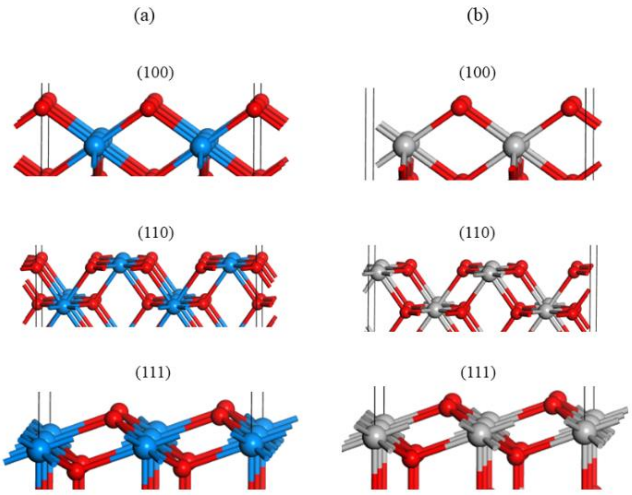

Fig. 1. Surface models of the (2×2) (100), (2×2) (110), and (2×2) (111) surfaces of the (a) UO_2 and (b) PuO_2 crystals. The surface structures shown are illustrative and not relaxed geometries. Blue and grey balls represent uranium and plutonium atoms, respectively, and red balls show oxygen atoms.

2. Materials and Methods

Ab initio atomistic thermodynamics approach was employed to conduct the surface energy phase diagram by plotting the surface free energy (γ^{ads}) as a function of the water chemical potential ($\Delta\mu_{H_2O}$). The surface free energy was computed for both molecular, dissociated water as well as a mixture of molecular-dissociated water over the low-index (100), (110), and (111) surfaces of UO_2 and PuO_2.

For surfaces in a water-rich environment, an exchange among surface adsorbed water species and those in the reservoir can occur under constant temperature, T, and pressure, p. The Gibbs free energy, G, is the key quantity to describe such an equilibrium system. It is a function of the number of Pu or U, N_x atoms and H_2O, N_{H_2O}, molecules as well as T and p.
The most stable adsorption configuration can be identified as the one which has minimum surface energy. The surface energy is defined as

$$\gamma^{ads} = \frac{1}{A}\left[\Delta G\left(T, p, N_x, N_{H_2O}\right) - \left(\Delta N_x \mu_x(T,p) + N_{H_2O}\mu_{H_2O}(T,p)\right)\right] \quad (1)$$

where ΔG is the difference in Gibbs energy between the adsorption system, which contains N_{H_2O} molecules,$G_{N_{H_2O}/slab}$, and the clean slab, $G_{clean\ slab}$

$$\Delta G = G_{N_{H_2O}/slab} - G_{clean\ slab} \quad (2)$$

μ_x and μ_{H_2O} are the chemical potentials of uranium or plutonium and molecular water, respectively, at certain T and p. The difference in the number of uranium or plutonium atoms between H_2O/UO_2 or H_2O/PuO_2 systems and the clean surface, ΔN_x, varies from zero only in the case of substitutional adsorption. Following the approach of previous researchers, the Gibbs free energy was approximated by the total energy of the system, *E*. Therefore, ΔG can be approximated as

$$\Delta G = E_{N_{H_2O}/slab} - E_{clean\ slab} \quad (3)$$

The reference point for μ_{H_2O} was determined to be the total energy of an isolated H_2O molecule, E_{H_2O}. Equation 1 can be, therefore, written as

$$\gamma^{ads} = \frac{1}{A}\left[E_{N_{H_2O}/slab} - E_{clean\ slab} - N_{H_2O}E_{H_2O} - \left(\Delta N_x \mu_x(T,p) + N_{H_2O}\left(\mu_{H_2O} - E_{H_2O}\right)(T,p)\right)\right] \quad (4)$$

The binding energy for a system contains N_{H_2O} molecules is defined as

$$E_{b_{(N_{H_2O})}} = \frac{1}{N_{H_2O}}\left[E_{N_{H_2O}/slab} - E_{clean\ slab} - N_{H_2O}E_{H_2O}\right] \quad (5)$$

Using the binding energy definition, with $\Delta N_x = 0$, Equation 4 can be shortened to

$$\gamma^{ads} = \frac{1}{A}\left[N_{H_2O}E_{b_{(N_{H_2O})}} - N_{H_2O}\Delta\mu_{H_2O}(T,p)\right] \quad (6)$$

The binding energy term, E_b, was obtained from the DFT results of Tegner et al.,(Tegner et al., 2017) who examined the adsorption of water on the low-index surfaces: (100), (110), and (111). These surfaces are commonly chosen for their thermodynamic stability and their status as the most representative facets of fluorite-structured actinide dioxides. The final exposed plane is consistently determined by low-index facets, as these crystal planes possess lower surface energies.(Zhao et al., 2024) Consequently, they are preferentially expressed in the final morphology in accordance with the Wulff structure.

Assuming the gaseous H_2O in the reservoir behaves as an ideal gas, the dependence of $\Delta\mu_{H_2O}$ on *T* and *p* is given by

$$\Delta\mu_{H_2O} = \tilde{\mu}_{H_2O}(T,p^o) + k_B T \ln\left(\frac{p_{H_2O}}{p^o}\right) \quad (7)$$

Where, $\tilde{\mu}_{H_2O}(T,p^o)$ is the chemical potential of H_2O at standard pressure (p^0), and temperature (T), k_B is the Boltzmann constant. Additional details on the approach are available in references.(Assaf et al., 2024; Bo et al., 2016; Munir et al., 2024; Reuter & Scheffler, 2001, 2003; Reuter et al., 2005; Suleiman et al., 2011a, 2011b; Suleiman et al., 2020; Zhang et al., 2021)

Results & Discussion

3.1. Stability of H_2O over UO_2 and PuO_2 (100) surfaces

Figure 2 depicts the surface free energies of different water configurations on the pristine UO_2 and PuO_2 (100) surfaces as a function of the water chemical potential, $\Delta\mu_{H_2O}$.

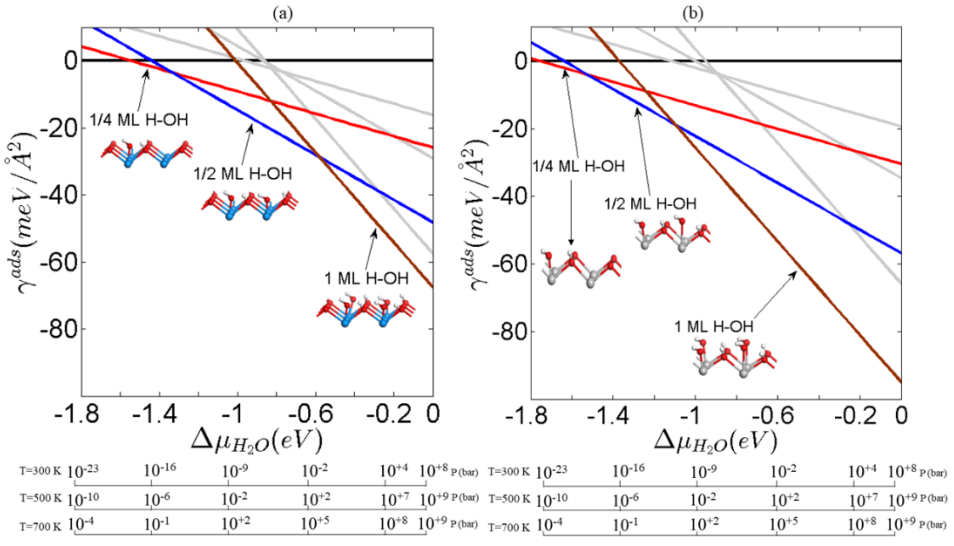

Fig. 2. Phase diagrams of surface energy for (a) $H_2O/UO_2(100)$ and (b) $H_2O/PuO_2(100)$ systems. Blue and Grey spheres denote U and Pu atoms, respectively. Red and white spheres signify oxygen and hydrogen atoms, respectively.

The applied coverage ranges from 1/4 ML to 1 ML for molecular and dissociative, H-OH, adsorptions. Only 1 ML coverage was applied for a configuration mixing 50 % molecular and 50% dissociative H-OH adsorption. **Figure 2 (a)** shows that for $\Delta\mu_{H_2O}$ < -1.50 eV, the clean UO_2(100) surface exhibits the maximum stability. Beyond the value $\Delta\mu_{H_2O} = -1.50$ eV, and within the interval -1.50 < $\Delta\mu_{H_2O}$ < -1.34 eV, the dissociative 1/4 ML structure emerges as the most stable configuration. As the chemical potential reaches the value -1.34 eV, the dissociative 1/2 ML structure is established as the most stable configuration; however, until the chemical potential value $\Delta\mu_{H_2O} = -0.60$ eV. Beyond $\Delta\mu_{H_2O} = -0.60$ eV and for the remaining range of the chemical potential, the dissociative 1 ML coverage is identified as the most stable configuration among all analyzed H_2O/UO_2(100) structures.

Figure 2 (b) shows that the clean PuO_2 surface has the highest stability at $\Delta\mu_{H_2O} < -1.80$ eV. At $\Delta\mu_{H_2O} = -1.80$ eV the dissociative 1/4 ML configuration becomes the most stable structure. The dissociative 1/2 ML phase becomes more dominant than 1/4 ML structure at $\Delta\mu_{H_2O} = -1.50$ eV; however, for the range -1.50 < $\Delta\mu_{H_2O}$ < -1.10 eV. Exceeding the value $\Delta\mu_{H_2O}$ = -1.10 eV, the dissociative 1 ML phase exhibits the highest stability for the remaining range of chemical potential.

A comparison of **Figures 2 (a) and (b)** demonstrates that water adsorption on PuO_2 is more advantageous than on UO_2. The initial stable dissociative structure at 1/4 ML was identified at $\Delta\mu_{H_2O} = -1.80$ eV for the PuO_2(100) surface, while $\Delta\mu_{H_2O}$ =-1.50 eV was seen for the first stable 1/4 ML dissociative phase on the UO_2(100) surface. The dissociative 1/2 ML phase attains greater stability at $\Delta\mu_{H_2O}$ values of -1.34 eV for UO_2 and -1.50 eV for PuO_2. In 1 ML dissociative configurations, stability was observed at $\Delta\mu_{H_2O}$values of -0.60 eV for UO_2 and -1.10 eV for PuO_2. These values confer an advantage to PuO_2 over UO_2 regarding water adsorption. This indicates that PuO_2 is more susceptible to surface hydration and reactivity with water than UO_2, potentially affecting corrosion resistance and shelf-life stability.

Figure 2 illustrates that dissociative adsorption structures dominate the stability for water interaction with both UO_2(100) and PuO_2(100) surfaces. This is in agreement with the results of Tegner et al.(Tegner et al., 2017). The 100 surfaces of UO_2 and PuO_2 are, therefore, anticipated to be fully hydroxylated, likely due to the reduced coordination of U and Pu at the surface, where hydroxyl groups facilitate stronger bonding and improved coordination relative to molecular water.

Figure 2 also presents a pressure scale at various temperatures (300 K, 500 K, and 700 K), linking our results to real temperature and pressure conditions. The pressure conditions corresponding to each temperature are presented in **Table 1** for the stable configurations of the H_2O/UO_2 and H_2O/PuO_2 systems. **Table 1** demonstrates that the dissociative 1 ML phase exhibits maximum stability under pressure settings that correspond to ambient and industrial environments, suggesting that 1 ML hydroxylated adsorption may be directly observable under these conditions for both UO_2 and PuO_2 surfaces.

Table 1. Water vapor pressures, p_{H_2O}, at 300 K, 500 K, and 700 K corresponding to $\Delta\mu_{H_2O}$ ranges for the most stable configurations of the H_2O/UO_2 (100) and H_2O/PuO_2 (100) systems.

	Structure	**$\Delta\mu_{H_2O}$ (eV)**	**Range of p (bar)**		
			300 K	**500 K**	**700 K**
UO_2	1/4 ML H-OH	$-1.50 < \Delta\mu_{H_2O} < -1.34$	10^{-18} - 10^{-15}	10^{-7} - 10^{-5}	10^{-2}- 10^{-1}
	1/2 ML H-OH	$-1.34 < \Delta\mu_{H_2O} < -0.60$	10^{-15} - 10^{-2}	10^{-5} – 10^{+2}	10^{-1} – 10^{+5}
	1 ML H-OH	$-0.60 < \Delta\mu_{H_2O}$	10^{-2} –10^{+8}	10^{+2} – 10^{+9}	10^{+5} – 10^{+9}
PuO_2	1/4 ML H-OH	$-1.80 < \Delta\mu_{H_2O} < -1.50$	10^{-23} - 10^{-18}	10^{-10} - 10^{-7}	10^{-4} - 10^{-2}
	1/2 ML H-OH	$-1.50 < \Delta\mu_{H_2O} < -1.10$	10^{-18} - 10^{-11}	10^{-7} - 10^{-3}	10^{-2} - 10^{+1}
	1 ML H-OH	$-0.10 < \Delta\mu_{H_2O}$	10^{-11} – 10^{+8}	10^{-3}– 10^{+9}	10^{+1}– 10^{+9}

2.2 Stability of H_2O over UO_2 and PuO_2(110) surfaces

The stability of various H_2O/UO_2(110) and H_2O/PuO_2(110) configurations is illustrated in **Figure 3**.

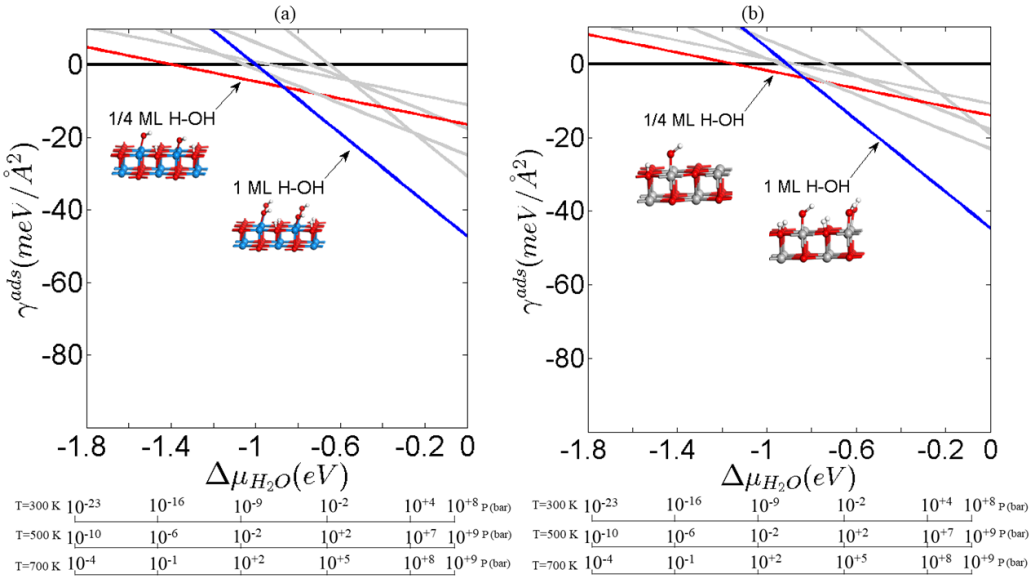

Fig. 3. Phase diagrams of surface energy of (a) H_2O/UO_2(110) and (b) H_2O/PuO_2(110) systems. Blue and Grey spheres denote U and Pu atoms, respectively. Red and white spheres signify oxygen and hydrogen atoms, respectively.

The applied coverages over the (110) surface are the same as those applied over the (100) index**. Figure 3 (a)** illustrates that the pristine UO_2(110) surface is the most stable configuration until the chemical potential attains the value $\Delta\mu_{H_2O} = -1.40$ eV, where the first H_2O/UO_2(110) system begins to demonstrate higher stability, with dissociative 1/4 ML configuration. This structure remains stable within the chemical potential range of $-1.40 \leq \Delta\mu_{H_2O} \leq -0.84$ eV. Beyond the value $\Delta\mu_{H_2O} = -0.84$ eV, the dissociative 1 ML structure emerges as the most stable configuration.

Figure 3 (b) elucidates the surface free energy of various H_2O/ PuO_2(110) structures. It shows that the dissociative 1/4 ML structure starts to be the most stable configuration at $\Delta\mu_{H_2O} = -1.19$ eV, and it remains like that within the range $-1.19 \leq \Delta\mu_{H_2O} \leq -0.81$ eV. Beyond $\Delta\mu_{H_2O} = -0.81$ eV, the dissociative 1 ML coverage is shown to be the most stable among all tested H_2O/PuO_2(110) structures.

The relationship between the most stable H_2O/UO_2 and H_2O/PuO_2 structures and the applied H_2O pressures conditions is illustrated in **Figure 3**, and summarized in **Table 2**. Similar to the observations with (100) surfaces, **Table 2** demonstrates that the dissociative 1 ML phase exhibits maximum stability under pressure settings that correspond to industrial operational conditions, suggesting that 1 ML hydroxylated adsorption may be directly observable under these conditions for both UO_2 and PuO_2(110) surfaces.

In contrast to the behavior of the (100) surfaces, the H_2O/UO_2 becomes more stable at $\Delta\mu_{H_2O} = -1.40$ and -0.84 eV for the dissociative 1/4 and 1 ML phases, respectively; whereas for H_2O/PuO_2 the dissociative 1/4 and 1 ML phases obtain stability at higher chemical potential values of $\Delta\mu_{H_2O} = -1.19$ and -0.81 eV, respectively. This suggests that UO_2(110) initiates hydroxylation at a lower pressure of water, and the PuO_2(110) exhibiting a marginal lack of reactivity with water compared to the UO_2(110) surface. This is in agreement with the findings of Jomard et al.(Jomard et al., 2014) and Zhang et al.(Zhang et al., 2018) who studied H_2O adsorption over the PuO_2(110) surface. Jomard et al.(Jomard et al., 2014) demonstrated that hydroxylated configurations become progressively more favorable with an increase in chemical potential. Their analysis indicated that the transition from the clean state to the dissociative 1/4 ML phase occurs around $\Delta\mu_{H_2O} = -1.3$ eV, while a dissociative 1 ML configuration is stabilized near $\Delta\mu_{H_2O} = -0.80$ eV. Their results also indicated that the PuO_2(110) surface is entirely saturated with hydroxyl groups at low temperatures, and the desorption is commenced between 300-400 K, depending on water pressure. However, they reported that the surface will be completely dry around 600-700 K. Zhang et al.(Zhang et al., 2018) investigated the dehydrating process on PuO_2(110) surface from first principles, revealing that water desorption occurs on the 1/4 ML, however, at very low water pressure. The abovementioned arguments validate the hydrophilic characteristics of PuO_2(110).

Table 2. Water vapor pressures, p_{H_2O}, at 300 K, 500 K, and 700 K corresponding to $\Delta\mu_{H_2O}$ ranges for the most stable configurations of the H_2O/UO_2 (110) and H_2O/PuO_2 (110) systems.

	Structure	$\Delta\mu_{H_2O}$ (eV)	Range of p (bar)		
			300 K	500 K	700 K
UO_2	1/4 ML H-OH	$-1.40 < \Delta\mu_{H_2O} < -0.84$	10^{-16} - 10^{-6}	10^{-6} - 1	10^{-1}- 10^{+3}
	1 ML H-OH	$-0.84 < \Delta\mu_{H_2O}$	10^{-6} –10^{+8}	1 – 10^{+9}	10^{+3} – 10^{+9}
PuO_2	1/4 ML H-OH	$-1.19 < \Delta\mu_{H_2O} < -0.81$	10^{-12} - 10^{-6}	10^{-3} - 1	10^{+1} - 10^{+3}
	1 ML H-OH	$-0.81 < \Delta\mu_{H_2O}$	10^{-6} – 10^{+8}	1– 10^{+9}	10^{+3}– 10^{+9}

2.3 Stability of H_2O over UO_2 and PuO_2(111) surfaces

Figure 4 (a) and (b) show the computed surface energy phase diagrams of various H_2O adsorption systems over the (111) surfaces of UO_2 and PuO_2, respectively.

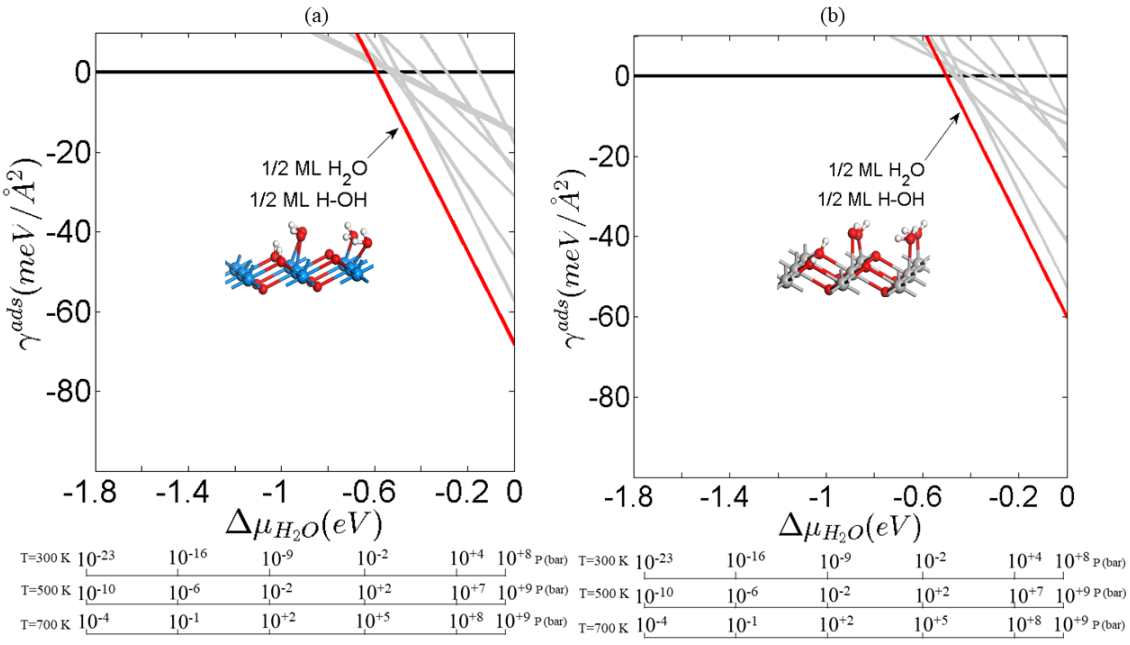

Fig. 4. Phase diagrams of surface energy of (a) H_2O/UO_2(111) and (b) H_2O/PuO_2(111) systems. Blue and Grey spheres denote U and Pu atoms, respectively. Red and white spheres signify oxygen and hydrogen atoms, respectively.

Figure 4 (a) reveals that only 1 ML mixture configuration, with 50% molecular and 50% dissociative adsorption, is the only stable phase among all investigated H_2O/UO_2(111) structures. It begins to exhibit stability at $\Delta\mu_{H_2O} = -0.6$ eV and for the whole range of chemical potential. **Figure 4 (b)** shows similar stable structures for H_2O/PuO_2(111) systems. The mixture 1 ML configuration is the only structure that has higher stability than the clean PuO_2(111) surface at $\Delta\mu_{H_2O} \geq -0.5$ eV. Tegner et al.(Tegner et al., 2017) Bo et al.(Bo et al., 2014) and Wellington et al.(Wellington et al., 2016) observed a significant resemblance between the surfaces of UO_2 and PuO_2, with the 50:50 mixed adsorption configuration demonstrating the most robust binding. They noted that the energy difference between the mixed and fully molecular adsorption modes is minimal (merely 0.07 eV), exhibiting narrow spectrum of adsorption energies. The augmented adsorption energy of the mixed configuration was attributed to the establishment of more robust

intramolecular hydrogen bonds on the (111) surfaces, which are preferable compared to those in the purely molecular adsorption scenario.(Tegner et al., 2017) The findings are also in agreement with those reported by Huang et al.(Huang et al., 2025) In their investigation of the chemisorption thermodynamics of O_2 and H_2O on the (110) and (111) surfaces of UO_2, they indicated that with increasing H_2O coverage, the adsorption mode of H_2O transitions from purely molecular adsorption to a mixed state including both molecular and dissociated species. This pattern was also reported by the DFT findings of Skomurski et al.(Skomurski et al., 2008) and Zhang et al.(Zhang et al., 2021). Skomurski et al.(Skomurski et al., 2008) examined the adsorption behavior of water and oxygen on the stable UO_2(111) surface. Their findings demonstrated that, at 1/2 ML coverage, molecular water adsorption is thermodynamically more advantageous than dissociative adsorption on a flawless surface. The presence of a surface defect may alter this preference, making dissociative adsorption more favorable, however, in this study, we only used the DFT results of Tegner et al.(Tegner et al., 2017), who studied the H_2O adsorption on a defect-free UO_2(111) surface. Zhang et al.(Zhang et al., 2021) assert in their study of the adsorption thermodynamics of H_2O and CO_2 on PuO_2(111) surface that the PuO_2(111) surface demonstrate considerable reactivity towards H_2O, facilitating rapid coverage by a mixed state of both molecular and dissociative species as the surface coverage increases, while CO_2 consistently maintains in a molecular adsorption state irrespective of coverage.

The clean UO_2(111) and PuO_2(111) surfaces maintain thermodynamically stable at $\Delta\mu_{H_2O}$ of -0.60 and -0.50 eV, respectively, resulting on PuO_2(111) has a stronger affinity to H_2O than UO_2(111). These chemical potentials equate to equilibrium pressures of 10^{-2} and 10^{-1} bar at 300 K, 10^{+2} , and 10^{+3} bar at 500 K, as well as 10^{+5} and 10^{+6} bar at 700 K. Beyond these levels, adsorption becomes advantageous (See **Table 3** below).

Table 3. Water vapor pressures, p_{H_2O}, at 300 K, 500 K, and 700 K corresponding to $\Delta\mu_{H_2O}$ ranges for the most stable configurations of the H_2O/UO_2 (111) and H_2O/PuO_2 (111) systems.

	Structure	$\Delta\mu_{H_2O}$ (eV)	Range of p (bar)		
			300 K	500 K	700 K
UO_2	1/2 ML H-OH 1/2 ML H_2O	$-0.6 < \Delta\mu_{H_2O}$	10^{-2} - 10^{+8}	10^{+2} - 10^{+9}	10^{+5}- 10^{+9}
PuO_2	1/4 ML H-OH 1/2 ML H_2O	$-0.5 < \Delta\mu_{H_2O}$	10^{-1} - 10^{+8}	10^{+3} - 10^{+9}	10^{+6} - 10^{+9}

Our reported results for H_2O/UO_2(111) are in agreement with the findings of Huang et al.(Huang et al., 2025) who showed that the accumulation of H_2O molecules progressively increased with rising pressure, aligning with the characteristics of multilayer adsorption.(Tegner & Kaltsoyannis, 2018) This confirms that H_2O exhibits monolayer and multilayer adsorption characteristics. Huang et al.(Huang et al., 2025) also found that at atmospheric pressure, the surface coverage of water molecules progressively diminishes, reaching 5.69 molecules/nm2 at 420K. Upon more heating, H_2O ultimately desorbs at 480 K.

2.4 The morphology of UO_2 and PuO_2 Nano-particles in a H_2O environment

The Wulff construction(Wulff, 1901) was employed to predict the equilibrium shapes of UO_2 and PuO_2 nanoparticles in a humid environment. The morphologies were constructed using WinXMorph software(Kaminsky, 2005, 2007) and utilizing the relative surface energies of the most stable H_2O/UO_2 and H_2O/PuO_2 systems over the low index surfaces as shown in **Figures 5(a) and 6(a)**, respectively.

Figure 5(b) shows the predicted shape of UO_2 nanoparticles over the spectrum of water chemical potentials $\Delta\mu_{H_2O}$. It illustrates that regardless of the $\Delta\mu_{H_2O}$, it was discovered that the (111) facet is the most prevalent, resulting in the nanoparticles having an octahedral form. Abramowski et al.(Abramowski et al., 1999) demonstrated same result for UO_2 nanoparticles via interatomic potential approaches. The equilibrium crystal shape is an octahedron predominantly bounded by (111) facets. **Figures 6(b) and (c)** show the calculated morphology of PuO_2 nanoparticles over the spectrum of water chemical potentials $\Delta\mu_{H_2O}$. It illustrates that the presence of PuO_2 in a humid environment forms an octahedral nanoparticle due to the domination of (111) facets for the whole chemical potential

spectra except for $\Delta\mu_{H_2O} = -0.50$ eV, where the (110) facets contribute to the Wulff constructions, resulting in truncated octahedral nanoparticles.

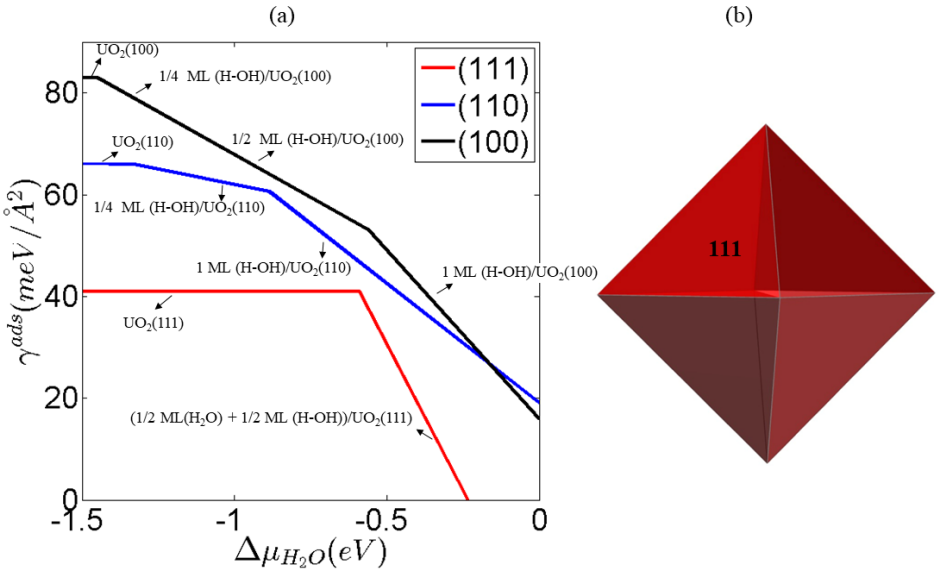

Fig. 5. Wulff construction of uranium oxides nanostructures in a humid environment. (a) Surface free energy of the most stable low-index UO_2(100), UO_2(110), and UO_2(111) surfaces as a function of water chemical potential. (b) Predicted UO_2 nanostructure morphologies regardless the chemical potential values of $\Delta\mu_{H_2O}$.

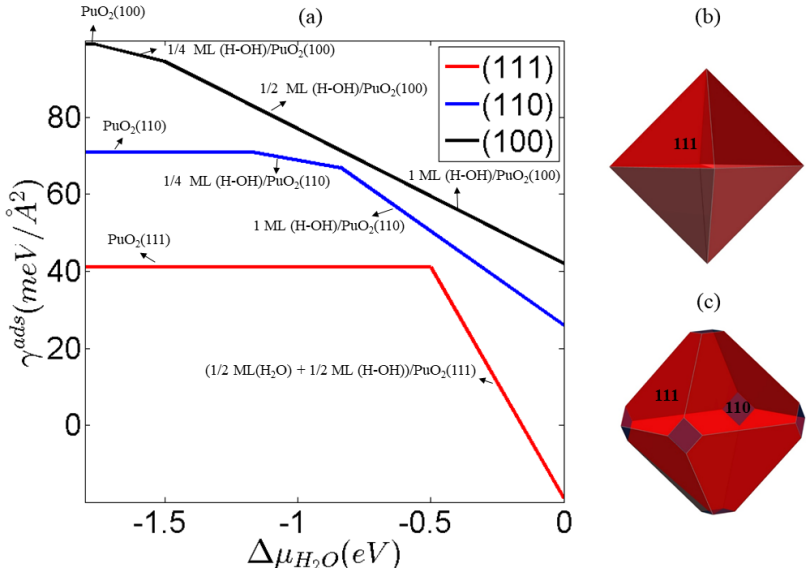

Fig. 6. Wulff construction of plutonium oxides nanostructures in a humid environment. (a) Surface free energy of the most stable low-index PuO_2(100), PuO_2(110), and PuO_2(111) surfaces as a function of water chemical potential. (b) Predicted PuO_2 nanostructure morphologies across all water chemical potential values, excluding $\Delta\mu_{H_2O} = -0.50$ eV. (c) Predicted PuO_2 nanostructure morphologies specifically at $\Delta\mu_{H_2O} = -0.50$ eV.

3. Conclusions

The constructed surface phase diagram for water adsorption on the low-index (100), (110), and (111) surfaces of UO_2 and PuO_2 reveal distinct stabilization patterns for molecular, dissociative (H-OH), and mixed adsorption configurations across varying water chemical potentials. The (100) surfaces of both oxides exhibit a sequential stabilization pattern, with UO_2 transitioning from 1/4 ML to 1/2 ML and 1 ML H-OH as hydration increased, while PuO_2 follows a similar sequence but with a stronger tendency for hydroxylation. On the (110) surfaces, UO_2 demonstrates earlier hydroxylation onset at lower water potentials, whereas PuO_2 stabilizes the 1/4 ML H-OH

phase over a broader range before achieving 1 ML coverage. The (111) surfaces stabilize mixed molecular-dissociative adsorption phases under elevated humidity, with PuO_2 showing greater affinity for surface hydration at lower water potentials.

The Wulff constructions derived from surface free energies suggest that both uranium and plutonium oxide nanoparticles tend to adopt geometries dominated by the thermodynamically stable (111) surfaces, even under varying water chemical potentials. Although hydration significantly lowers the surface energies of the (100) and (110) facets, particularly for PuO_2, these changes are not sufficient to disrupt the overall shape, which remains largely octahedral. Notably, under specific humid conditions, such as at $\Delta\mu_{H_2O} = -0.50$ eV, the inclusion of (110) facets in PuO_2 alters the morphology toward a truncated octahedron. This suggests that hydration modifies surface stability without significantly altering nanoparticle geometry, while simultaneously increasing the probability of (100) and (110) surface exposure and reactivity in practical conditions.

These findings provide essential insights into the surface chemistry and morphological development of actinide oxides under humid environments, directly impacting nuclear fuel reprocessing, long-term storage safety, and corrosion resistance in confinement environments. This work enhances the basic comprehension of water–actinide surface interactions, hence aiding in the predictive modeling of material behavior in nuclear systems and facilitating the formulation of solutions to mitigate environmental dangers linked to radioactive waste management.

4. Recommendation for future work

Subsequent research should prioritize expanding water adsorption studies beyond ideal stoichiometric surfaces to include more realistic models that integrate grain boundaries, surface reconstructions, and defect clusters, which are often seen in nuclear fuel and storage materials. Investigating the influencing of dopants (e.g., Gd, Zr, or Ce) on the energetics of water adsorption may facilitate the development of corrosion-resistant or catalytically active mixed oxides.

CRediT Author Contribution Statement

N. W. Assaf: Conceptualization, Methodology, Formal analysis, Investigation, Resources, Data curation, Writing-original draft, Writing – Review & Editing, Visualization, Supervision.
I. Oluwoye: Writing – Review & Editing, Visualization.
A. Marashdeh: Writing – Review & Editing, Visualization, Funding Acquisition.
A. Elrashidi: Writing – Review & Editing, Visualization, Funding Acquisition.

Declaration Statements

Conflicts of Interest
The authors declare no conflict of interest.

Nomenclature

Symbol	Description	Unit
A	Surface Area	[Å^2]
E_b	Binding energy	[eV]
k	Boltzman Costant	[eV/K]
ML	Monolayer	[-]
N_{H_2O}	Number of water molecules	[-]
P	Pressure	[bar]
p^0	Standard Pressure	[bar]
T	Temperature	[K]
γ^{ads}	Surface free energy	[meV/Å^2]

Symbol	Description	Unit
μ_{H_2O}	water chemical potential	eV

References

Abramowski, M., Grimes, R. W., & Owens, S. (1999). Morphology of UO_2. *Journal of Nuclear Materials*, *275*(1), 12-18. https://doi.org/10.1016/S0022-3115(99)00110-5

Ao, B., Lu, H., Qiu, R., Ye, X., Shi, P., Chen, P., & Wang, X. (2015). First-Principles Energetics of Some Nonmetallic Impurity Atoms in Plutonium Dioxide. *The Journal of Physical Chemistry C*, *119*(27), 14879-14889. https://doi.org/10.1021/acs.jpcc.5b02276

Assaf, N., Suleiman, I., & Malkawi, B. (2024). The Equilibrium stability of CH_4 and CO_2 on the calcite (10.4) surface: An atomistic thermodynamics investigation. *Jordanian Journal of Engineering and Chemical Industries*, *7*(1), 1-4. https://doi.org/10.48103/jjeci712024

Baker, M. M., Less, L. N., & Orman, S. (1966). Uranium + water reaction. Part 1.—Kinetics, products and mechanism [10.1039/TF9666202513]. *Transactions of the Faraday Society*, *62*(0), 2513-2524. https://doi.org/10.1039/TF9666202513

Balooch, M., & Hamza, A. V. (1996). Hydrogen and water vapor adsorption on and reaction with uranium. *Journal of Nuclear Materials*, *230*(3), 259-270. https://doi.org/10.1016/0022-3115(96)80023-7

Banos, A., Burrows, R., & Scott, T. B. (2021). A review of the mechanisms, reaction products and parameters affecting uranium corrosion in water. *Coordination Chemistry Reviews*, *439*, 213899. https://doi.org/10.1016/j.ccr.2021.213899

Banos, A., Harker, N. J., & Scott, T. B. (2018). A review of uranium corrosion by hydrogen and the formation of uranium hydride. *Corrosion Science*, *136*, 129-147. https://doi.org/10.1016/j.corsci.2018.03.002

Banos, A., & Scott, T. B. (2020). A review of the reaction rates of uranium corrosion in water. *Journal of Hazardous Materials*, *399*, 122763. https://doi.org/10.1016/j.jhazmat.2020.122763

Bo, T., Lan, J.-H., Zhao, Y.-L., Zhang, Y.-J., He, C.-H., Chai, Z.-F., & Shi, W.-Q. (2014). First-principles study of water adsorption and dissociation on the UO_2 (111), (110) and (100) surfaces. *Journal of Nuclear Materials*, *454*(1), 446-454. https://doi.org/10.1016/j.jnucmat.2014.09.001

Bo, T., Lan, J.-H., Zhao, Y.-L., Zhang, Y.-J., He, C.-H., Chai, Z.-F., & Shi, W.-Q. (2016). Surface properties of NpO_2 and water reacting with stoichiometric and reduced NpO_2 (111), (110), and (100) surfaces from ab initio atomistic thermodynamics. *Surface Science*, *644*, 153-164. https://doi.org/10.1016/j.susc.2015.09.016

Cozzo, C., Staicu, D., Somers, J., Fernandez, A., & Konings, R. J. M. (2011). Thermal diffusivity and conductivity of thorium–plutonium mixed oxides. *Journal of Nuclear Materials*, *416*(1), 135-141. https://doi.org/10.1016/j.jnucmat.2011.01.109

Cui, D., Low, J., & Spahiu, K. (2011). Environmental behaviors of spent nuclear fuel and canister materials [10.1039/C0EE00582G]. *Energy & Environmental Science*, *4*(7), 2537-2545. https://doi.org/10.1039/C0EE00582G

Donald, S. B., Davisson, M. L., & Nelson, A. J. (2016). XPS Investigation on Changes in UO_2 Speciation following Exposure to Humidity. *MRS Advances*, *1*(44), 2993-2997. https://doi.org/10.1557/adv.2016.286

Eriksen, T. E., Shoesmith, D. W., & Jonsson, M. (2012). Radiation induced dissolution of UO_2 based nuclear fuel – A critical review of predictive modelling approaches. *Journal of Nuclear Materials*, *420*(1), 409-423. https://doi.org/10.1016/j.jnucmat.2011.10.027

Flores, H. G. G., Roussel, P., Moore, D. P., & Pugmire, D. L. (2011). Characterization and stability of thin oxide films on plutonium surfaces. *Surface Science*, *605*(3), 314-320. https://doi.org/10.1016/j.susc.2010.10.034

Gibby, R. L. (1971). The effect of plutonium content on the thermal conductivity of (U, Pu)O_2 solid solutions. *Journal of Nuclear Materials*, *38*(2), 163-177. https://doi.org/10.1016/0022-3115(71)90040-7

Haschke, J. M. (1998). Corrosion of uranium in air and water vapor: consequences for environmental dispersal. *Journal of Alloys and Compounds*, *278*(1), 149-160. https://doi.org/10.1016/S0925-8388(98)00639-2

Haschke, J. M., Allen, T. H., & Morales, L. A. (2000). Reaction of Plutonium Dioxide with Water: Formation and Properties of PuO_{2+x}. *Science*, *287*(5451), 285-287. https://doi.org/10.1126/science.287.5451.285

Haschke, J. M., Allen, T. H., & Morales, L. A. (2001). Reactions of plutonium dioxide with water and hydrogen–oxygen mixtures: Mechanisms for corrosion of uranium and plutonium. *Journal of Alloys and Compounds*, *314*(1), 78-91. https://doi.org/10.1016/S0925-8388(00)01222-6

Haschke, J. M., & Ricketts, T. E. (1997). Adsorption of water on plutonium dioxide. *Journal of Alloys and Compounds*, *252*(1), 148-156. https://doi.org/10.1016/S0925-8388(96)02627-8

Hausner, H. (1965). Determination of the melting point of uranium dioxide. *Journal of Nuclear Materials*, *15*(3), 179-183. https://doi.org/10.1016/0022-3115(65)90178-9

Hedhili, M. N., Yakshinskiy, B. V., & Madey, T. E. (2000). Interaction of water vapor with UO_2(001). *Surface Science*, *445*(2), 512-525. https://doi.org/10.1016/S0039-6028(99)01117-6

Hernandez, S. C., & Holby, E. F. (2016). DFT+U Study of Chemical Impurities in PuO_2. *The Journal of Physical Chemistry C*, *120*(24), 13095-13102. https://doi.org/10.1021/acs.jpcc.6b03469

Huang, Y., Zhang, L., Ji, H., Zhang, Z., Zhang, Q., Sun, B., Song, H. (2025). The chemisorption thermodynamics of O_2 and H_2O on AFM UO_2 surfaces unraveled by DFT+ U-D3 study. *arXiv preprint arXiv:2502.08078*. https://doi.org/10.48550/arXiv.2502.08078

Jomard, G., Bottin, F., & Geneste, G. (2014). Water adsorption and dissociation on the PuO_2(110) surface. *Journal of Nuclear Materials*, *451*(1), 28-34. https://doi.org/10.1016/j.jnucmat.2014.03.012

Jonsson, M., Nielsen, F., Roth, O., Ekeroth, E., Nilsson, S., & Hossain, M. M. (2007). Radiation Induced Spent Nuclear Fuel Dissolution under Deep Repository Conditions. *Environmental Science & Technology*, *41*(20), 7087-7093. https://doi.org/10.1021/es070832y

Kaminsky, W. (2005). WinXMorph: a computer program to draw crystal morphology, growth sectors and cross sections with export files in VRML V2. 0 utf8-virtual reality format. *Applied Crystallography*, *38*(3), 566-567. https://doi.org/10.1107/S0021889805012148

Kaminsky, W. (2007). From CIF to virtual morphology using the WinXMorph program. *Applied Crystallography*, *40*(2), 382-385. https://doi.org/10.1107/S0021889807003986

Kurosaki, K., Yamada, K., Uno, M., Yamanaka, S., Yamamoto, K., & Namekawa, T. (2001). Molecular dynamics study of mixed oxide fuel. *Journal of Nuclear Materials*, *294*(1), 160-167. https://doi.org/10.1016/S0022-3115(01)00451-2

Lucuta, P. G., Matzke, H., & Hastings, I. J. (1996). A pragmatic approach to modelling thermal conductivity of irradiated UO2 fuel: Review and recommendations. *Journal of Nuclear Materials*, *232*(2), 166-180. https://doi.org/10.1016/S0022-3115(96)00404-7

Maldonado, P., Evins, L. Z., & Oppeneer, P. M. (2014). Ab Initio Atomistic Thermodynamics of Water Reacting with Uranium Dioxide Surfaces. *The Journal of Physical Chemistry C*, *118*(16), 8491-8500. https://doi.org/10.1021/jp501715m

Manner, W. L., Lloyd, J. A., & Paffett, M. T. (1999). Reexamination of the fundamental interactions of water with uranium. *Journal of Nuclear Materials*, *275*(1), 37-46. https://doi.org/10.1016/S0022-3115(99)00100-2

McEachern, R. J., & Taylor, P. (1998). A review of the oxidation of uranium dioxide at temperatures below 400°C. *Journal of Nuclear Materials*, *254*(2), 87-121. https://doi.org/10.1016/S0022-3115(97)00343-7

Munir, S., Ta, K. M., Smith, T., Gillie, L. J., Cooke, D. J., Parker, S. C., & Molinari, M. (2024). Strain Effects on the Adsorption of Water on Cerium Dioxide Surfaces and Nanoparticles: A Modeling Outlook. *The Journal of Physical Chemistry C*, *128*(43), 18451-18464. https://doi.org/10.1021/acs.jpcc.4c04172

Pacchioni, G. (2017). Surface reconstructions: Polaron bricklayers at work. *Nature Reviews Materials*, *2*(11), 17071. https://doi.org/10.1038/natrevmats.2017.71

Paffett, M. T., Kelly, D., Joyce, S. A., Morris, J., & Veirs, K. (2003). A critical examination of the thermodynamics of water adsorption on actinide oxide surfaces. *Journal of Nuclear Materials*, *322*(1), 45-56. https://doi.org/10.1016/S0022-3115(03)00315-5

Pang, J. W. L., Buyers, W. J. L., Chernatynskiy, A., Lumsden, M. D., Larson, B. C., & Phillpot, S. R. (2013). Phonon Lifetime Investigation of Anharmonicity and Thermal Conductivity of UO_2 by Neutron Scattering and Theory. *Physical Review Letters*, *110*(15), 157401. https://doi.org/10.1103/PhysRevLett.110.157401

Papageorgiou, A. C., Beglitis, N. S., Pang, C. L., Teobaldi, G., Cabailh, G., Chen, Q.,…Thornton, G. (2010). Electron traps and their effect on the surface chemistry of TiO_2(110). *Proceedings of the National Academy of Sciences*, *107*(6), 2391-2396. https://doi.org/doi:10.1073/pnas.0911349107

Prodan, I. D., Scuseria, G. E., & Martin, R. L. (2006). Assessment of metageneralized gradient approximation and screened Coulomb hybrid density functionals on bulk actinide oxides. *Physical Review B*, *73*(4), 045104. https://doi.org/10.1103/PhysRevB.73.045104

Reticcioli, M., Setvin, M., Hao, X., Flauger, P., Kresse, G., Schmid, M.,…Franchini, C. (2017). Polaron-Driven Surface Reconstructions. *Physical Review X*, *7*(3), 031053. https://doi.org/10.1103/PhysRevX.7.031053

Reuter, K., & Scheffler, M. (2001). Composition, structure, and stability of RuO_2(110) as a function of oxygen pressure. *Physical Review B*, *65*(3), 035406. https://doi.org/10.1103/PhysRevB.65.035406

Reuter, K., & Scheffler, M. (2003). First-Principles Atomistic Thermodynamics for Oxidation Catalysis: Surface Phase Diagrams and Catalytically Interesting Regions. *Physical Review Letters*, *90*(4), 046103. https://doi.org/10.1103/PhysRevLett.90.046103

Reuter, K., Stampf, C., & Scheffler, M. (2005). AB Initio Atomistic Thermodynamics and Statistical Mechanics of Surface Properties and Functions. In S. Yip (Ed.), *Handbook of Materials Modeling: Methods* (pp. 149-194). Springer Netherlands. https://doi.org/10.1007/978-1-4020-3286-8_10

Richmond, S., Bridgewater, J. S., Ward, J. W., & Allen, T. H. (2010). The solubility of hydrogen and deuterium in alloyed, unalloyed and impure plutonium metal. *IOP Conference Series: Materials Science and Engineering*, *9*(1), 012036. https://doi.org/10.1088/1757-899X/9/1/012036

Ritchie, A. G. (1981). A review of the rates of reaction of uranium with oxygen and water vapour at temperatures up to 300°c. *Journal of Nuclear Materials*, *102*(1), 170-182. https://doi.org/https://doi.org/10.1016/0022-3115(81)90557-2

Senanayake, S. D., & Idriss, H. (2004). Water reactions over stoichiometric and reduced UO_2(111) single crystal surfaces. *Surface Science*, *563*(1), 135-144. https://doi.org/10.1016/j.susc.2004.06.169

Senanayake, S. D., Rousseau, R., Colegrave, D., & Idriss, H. (2005). The reaction of water on polycrystalline UO2: Pathways to surface and bulk oxidation. *Journal of Nuclear Materials*, *342*(1), 179-187. https://doi.org/10.1016/j.jnucmat.2005.04.060

Skomurski, F. N., Shuller, L. C., Ewing, R. C., & Becker, U. (2008). Corrosion of UO_2 and ThO_2: A quantum-mechanical investigation. *Journal of Nuclear Materials*, *375*(3), 290-310. https://doi.org/10.1016/j.jnucmat.2007.12.007

Stakebake, J. L. (1971). The storage behavior of plutonium metal, alloys, and oxide: A review. *Journal of Nuclear Materials*, *38*(3), 241-259. https://doi.org/10.1016/0022-3115(71)90054-7

Stultz, J., Paffett, M. T., & Joyce, S. A. (2004). Thermal Evolution of Hydrogen Following Water Adsorption on Defective UO_2(100). *The Journal of Physical Chemistry B*, *108*(7), 2362-2364. https://doi.org/10.1021/jp031066u

Suleiman, I. A., Radny, M. W., Gladys, M. J., Smith, P. V., Mackie, J. C., Kennedy, E. M., & Dlugogorski, B. Z. (2011a). Chlorination of the Cu(110) Surface and Copper Nanoparticles: A Density Functional Theory Study. *The Journal of Physical Chemistry C*, *115*(27), 13412-13419. https://doi.org/10.1021/jp2036372

Suleiman, I. A., Radny, M. W., Gladys, M. J., Smith, P. V., Mackie, J. C., Kennedy, E. M., & Dlugogorski, B. Z. (2011b). An equilibrium ab initio atomistic thermodynamics study of chlorine adsorption on the Cu(001) surface [10.1039/C0CP02211J]. *Physical Chemistry Chemical Physics*, *13*(21), 10306-10311. https://doi.org/10.1039/C0CP02211J

Suleiman, I. A., Shawaqfeh, A. T., Stockenhuber, M., & Kennedy, E. M. (2020). Insights on the stability of cuprous chloride under high pressure: An equilibrium ab initio atomistic thermodynamics study. *Journal of Physics and Chemistry of Solids*, *136*, 109158. https://doi.org/10.1016/j.jpcs.2019.109158

Tegner, B. E., & Kaltsoyannis, N. (2018). Multiple water layers on AnO_2 {111}, {110}, and {100} surfaces (An = U, Pu): A computational study. *Journal of Vacuum Science & Technology A*, *36*(4). https://doi.org/10.1116/1.5028210

Tegner, B. E., Molinari, M., Kerridge, A., Parker, S. C., & Kaltsoyannis, N. (2017). Water Adsorption on AnO_2 {111}, {110}, and {100} Surfaces (An = U and Pu): A Density Functional Theory + U Study. *The Journal of Physical Chemistry C*, *121*(3), 1675-1682. https://doi.org/10.1021/acs.jpcc.6b10986

Tian, X.-f., Wang, H., Xiao, H.-x., & Gao, T. (2014). Adsorption of water on UO_2 (111) surface: Density functional theory calculations. *Computational Materials Science*, *91*, 364-371. https://doi.org/10.1016/j.commatsci.2014.05.009

Vălu, O. S., Staicu, D., Beneš, O., Konings, R. J. M., & Lajarge, P. (2014). Heat capacity, thermal conductivity and thermal diffusivity of uranium–americium mixed oxides. *Journal of Alloys and Compounds*, *614*, 144-150. https://doi.org/10.1016/j.jallcom.2014.05.083

Wang, G., Batista, E. R., & Yang, P. (2019). Excess Electrons on Reduced AnO_2 (111) Surfaces (An = Th, U, Pu) and Their Impacts on Catalytic Water Splitting. *The Journal of Physical Chemistry C*, *123*(50), 30245-30251. https://doi.org/10.1021/acs.jpcc.9b06543

Wasywich, K. M., Hocking, W. H., Shoesmith, D. W., & Taylor, P. (1993). Differences in Oxidation Behavior of Used CANDU Fuel During Prolonged Storage in Moisture-Saturated Air and Dry Air at 150°C. *Nuclear Technology*, *104*(3), 309-329. https://doi.org/10.13182/NT93-A34893

Wellington, J. P. W., Kerridge, A., Austin, J., & Kaltsoyannis, N. (2016). Electronic structure of bulk AnO_2 (An = U, Np, Pu) and water adsorption on the (111) and (110) surfaces of UO_2 and PuO_2 from hybrid density functional theory within the periodic electrostatic embedded cluster method. *Journal of Nuclear Materials*, *482*, 124-134. https://doi.org/10.1016/j.jnucmat.2016.10.005

Wulff, G. (1901). On the question of speed of growth and dissolution of crystal surfaces. *Z. Kristallogr*, *34*(5/6), 449. https://doi.org/10.1524/zkri.1901.34.1.449

Yim, C. M., Chen, J., Zhang, Y., Shaw, B.-J., Pang, C. L., Grinter, D. C., Thornton, G. (2018). Visualization of Water-Induced Surface Segregation of Polarons on Rutile TiO_2(110). *The Journal of Physical Chemistry Letters*, *9*(17), 4865-4871. https://doi.org/10.1021/acs.jpclett.8b01904

Zhang, C., Yang, Y., & Zhang, P. (2018). Thermodynamics Study of Dehydriding Reaction on the PuO_2(110) Surface from First Principles. *The Journal of Physical Chemistry C*, *122*(14), 7790-7794. https://doi.org/10.1021/acs.jpcc.8b01414

Zhang, L., Sun, B., Zhang, Q., Liu, H., Liu, K., & Song, H. (2021). The adsorption thermodynamics of H_2O and CO_2 on PuO_2(111) surface: A comparative study based on DFT+U-D3. *Applied Surface Science*, *537*, 147882. https://doi.org/10.1016/j.apsusc.2020.147882

Zhao, Y., Zhang, W., Sun, L., Li, X., Deng, W., & Zhang, L. (2024). Wulff Constructions for an Equilibrium MFI-Type Zeolite Shape Modelling under Different Conditions. *Crystals*, *14*(1), 63. https://doi.org/10.3390/cryst14010063